International Journal of Greenhouse Gas Control 150 (2026) 104578

Contents lists available at ScienceDirect

International Journal of Greenhouse Gas Control

journal homepage: www.elsevier.com/locate/ijggc

Assessment of prospective CO_2 geological storage resources in the Taiwan Strait

Jianghui Li [a,b,c,*], Yanni Hou [a], Fengling Yu [a,b,**], Daolong Zhou [a], Hengnian Dong [a], Xiaokang Zhang [a,c]

[a] College of Ocean and Earth Sciences, Xiamen University, Xiamen, Fujian, China
[b] State Key Laboratory of Marine Environmental Science, Xiamen University, Xiamen, Fujian, China
[c] Key Laboratory of Underwater Acoustic Communication and Marine Information Technology, Ministry of Education, Xiamen, Fujian, China

ARTICLE INFO

Keywords:
Sag-scale
Resources assessment
Taixi basin
Carbon dioxide
Geological storage
Pressure limitations

ABSTRACT

Geological storage of carbon dioxide (CO_2) is a viable option for achieving large-scale and cost-effective reduction in global CO_2 emissions. The Taixi Basin, spanning the Taiwan Strait, is a potential storage field for reducing CO_2 emissions in the Fujian and Taiwan regions. It hosts multiple effective reservoir-seal combinations, with abundant sandstone formations. These combinations divide the Taixi Basin into five dominant sags, namely the Taizhong Sag, Xinzhu Sag, Jiulongjiang Sag, Jinjiang Sag, and Chongwu Sag. However, the resource assessment of CO_2 storage in the Taixi Basin is typically conducted at the basin-scale, which makes it difficult to determine the resources of the target areas with optimal burial depths and superior reservoir conditions. This study estimates the prospective CO_2 storage resources for each sag of the Taixi Basin using DOE volumetric methods, both without and with considering the pressure limitations. This approach allows for a more in-depth and accurate characterization of regional storage resources. The results show that the theoretical storage resources of the Taixi Basin range between 16.3 Gt and 62.2 Gt, and the effective resources range between 5.03 Gt and 12.3 Gt. This not only provides a clear range of theoretical and effective storage resources but also serves as a guide for implementing real-world CO_2 storage projects.

1. Introduction

With the excessive emission of carbon dioxide (CO_2), the greenhouse effect has intensified significantly, making global climate change one of the most pressing environmental challenges (Michael et al., 2010; Goodman et al., 2013). To slow down the CO_2 emission into the atmosphere, carbon capture, utilization, and storage (CCUS) has been regarded as a key methodology (Wang et al., 2022; Xie and Huang, 2003), which involves extensive research on CO_2 geological storage onshore and offshore (Xie and Huang, 2003; Cao and Chen, 2022). The principle of the CO_2 storage involves injecting captured and isolated CO_2 into suitable geological formations, including saline aquifers or depleted hydrocarbon reservoirs, where the depth is normally larger than 800 meters (Bachu et al., 2007; Schrag, 2009; Bachu and Shaw, 2003; Jiang et al., 2008). Such circumstance can exceed the critical conditions for supercritical CO_2, which is 31.1 °Celsius and 7.38 MPa.

Over the past decades, China's economy has been increasingly growing, and the CO_2 emissions from China's coastal regions have also been steadily increasing. For supporting China's goal of carbon neutrality, the implementation of CCUS is vital, and the deep saline aquifers present substantial storage potential (Li, 2025; Su et al., 2021; Qin et al., 2012; Guo et al., 2011, 2015a; Diao et al., 2021). However, the onshore part of these regions has been proven unsuitable for large-scale long-term CO_2 storage due to their limited spatial extent, poor reservoir quality, and high population density in adjacent regions (Diao et al., 2021; Li, 2025). In contrast, China's offshore areas contain numerous large sedimentary basins with substantial sediment thickness (typically exceeding 1000 m) (Diao et al., 2021), well-developed reservoir-caprock systems, abundant structural traps, and favorable geological conditions for CO_2 storage. It encompasses areas such as the East China Sea Shelf Basin, Pearl River Mouth Basin, South Yellow Sea Basin, Bohai Bay Basin, Taixi Basin, etc. These basins feature relatively thick sedimentary layers and suitable closed conditions. It was estimated that the theoretical storage potential of China's coastal sedimentary basins can reach thousands of billions of tonnes of CO_2 (Li et al., 2016). For instance, Huo (Huo, 2014) estimated 11 China's offshore major sedimentary basins and yielded a total basin-scale potential of 2500 Gt. Chen et al.

* Correspondence to: Xiping Building C3-201, Xiamen University, Xiangan, Xiamen, Fujian, China.
** Corresponding author.
E-mail addresses: jli@xmu.edu.cn (J. Li), fengling.yu@xmu.edu.cn (F. Yu).

https://doi.org/10.1016/j.ijggc.2026.104578
Received 19 July 2025; Received in revised form 1 December 2025; Accepted 13 January 2026
Available online 21 January 2026

(2024) evaluated 18 major sedimentary basins in Chinese maritime territories and yielded a total basin-scale potential of 2580 Gt. Zhou et al. (2011) conducted basin-scale assessments specifically for the Pearl River Mouth Basin with the storage resources of 308 Gt. However, these assessments are predominantly at the basin scale, which often overlooks critical local heterogeneities that are essential for practical engineering applications.

China is now planning large-scale marine carbon storage projects in the South China Sea and the Bohai Sea. In contrast, research in the Taiwan Strait lacks both integrity and systematization, mainly because of the limited geological exploration data. The Taixi Basin (Fig. 1), located between the Fuzhou-Xiamen connection line and Taiwan's Central Mountain Range, which includes the Taiwan Strait and western Taiwan Island Fu et al. (2012), is a Mesozoic-Cenozoic sedimentary basin and one of China's largest offshore Cenozoic hydrocarbon-bearing basins. It is characterized by multiple sandstone reservoirs with porosity exceeding 15%, regional mudstone caprocks thicker than 50 m, and stable tectonic conditions since the Pliocene. These features create favorable conditions for CO_2 geological storage, making the basin a critical geological reservoir for cross-strait carbon storage, demonstrating significant resource advantages in accommodating industrial emissions from Taiwan (287 million tons annually) (Tai, 2023) and Fujian (295 million tons annually) (Fuj, 2023).

Previously, the storage resources of CO_2 storage for the Taixi Basin have been partially investigated. Jiao (2014) estimated the total effective CO_2 storage resources of 12.5 Gt CO_2 under the effective Taiwan Strait and coastal plain, which mainly consists of Taizhong and Xinzhu Sags, and the constructed three–dimensional (3D) geological model with main geological features, which simplified the complex geological conditions. Yu et al. (2017) studied three deep reservoirs in the Taixi Basin with a total effective storage resource of about 13.7 Gt CO_2. Lin et al. (2023) divided the Taixi Basin into 20 km × 20 km squares, showing the distribution of CO_2 storage in each block of the deep saline aquifer in Taiwan, and estimated the carbon storage resources of the terrestrial and deep saline aquifer in the Taixi Basin to be 39 Gt. The adoption of conservative geological condition screening criteria (such as excluding areas with too shallow burial depth or unstable structure) has led to a significant reduction in the estimated effective resource volume compared to the theoretical resource volume. In addition, these results vary widely mainly because of an under-representative research area (e.g., concentrated in the coastal area of Taiwan) or selected cores.

This study uses comprehensive data from drilling and seismic profiles (Table 1) to explore the theoretical resources of CO_2 storage in the Taixi Basin at the sag-scale, with state-of-the-art data, such as from the drilling wells and the seismic profile. In the investigation, we consider the stratigraphy, geological conditions, reservoir-caprock characteristics, and hydrogeological conditions for each sag in the Basin. These sags are Taizhong Sag, Xinzu Sag, Jiulongjiang Sag, Jinjiang Sag, and Chongwu Sag. We develop the stratigraphy of each sag reservoir caprock in 3D. By evaluating the storage potential of individual sag units, the research provides technical support for subsequent potential assessments, target zone identification, site selection, and demonstration project development. This study will be the first comprehensive, sag-scale CO_2 storage assessment specifically targeting the Taixi Basin, and the sag-scale methodology represents a significant advancement over traditional basin-scale evaluations. By deconstructing the basin into its fundamental tectonic units (sags), we provide a spatially explicit resource characterization. To estimate the theoretical and effective resources of the Taixi Basin, we consider the pressure limitations.

This paper is organized as follows. Section 2 demonstrates the methodologies of this study. Section 3 details the geological and hydrological settings of the Taixi Basin. Section 4 presents the assessment of storage potential for each sag. In Section 5, conclusions are summarized and discussed.

2. Methodology

For storage resources assessment, we first identify individual reservoirs in each sag and assess their 3D spatial coverage. Then we apply the presented assessment method on each reservoir to calculate the theoretical storage resources, and finally integrate these individual resources into the entire basin. We use a comprehensive evaluation framework to estimate the CO_2 geological storage potential of the Taixi Basin. Fig. 2 shows the processes of CO_2 storage resources assessment in the Taixi Basin. First, we use the volumetric method to calculate the theoretical storage resources of the basin. Subsequently, to better align with the actual engineering conditions, we introduce pressure limitations to assess the amount of effectively contained resources within the safe pressure window. Finally, the calculation results of the two methods are comparatively analyzed to provide a comprehensive perspective on resource evaluation. Moreover, the calculation results are analyzed probabilistically (i.e., P_{10}, P_{50}, and P_{90}) by surveying the parameters, including reservoir effective thickness, porosity, supercritical CO_2 density, and storage efficiency factor.

2.1. Sag-scale storage spatial identification

Fig. 3 shows the calculation of the specific sandstone volume unit. The sandstone reservoir volumetric assessment employs a stratigraphy-based geometric approach integrating drilling well data and seismic profiles, initiated with vertical thickness measurement where sandstone thickness (h_{sand}) is derived from well logs and lithological descriptions of exploration wells such as Well PA (Hsiao et al., 1991b) (Fig. 1), followed by stratigraphic calibration that correlates identified formation boundaries, including sandstone tops and unconformities, to corresponding seismic reflectors, while the lateral distribution of sandstone bodies (L_{sand}) along depositional strike and dip directions is determined through integrated seismic facies interpretation, inter-well correlation profiles, and formation-by-formation stratigraphic analysis to achieve a comprehensive 3D reservoir characterization.

In this study, the offshore geological storage potential of the five major sags in the Taixi Basin is evaluated, and the reservoir caprock strata are analyzed according to the existing profiles and drilling wells in each sag. The sandstone content of different strata is evaluated to obtain the storage resources of the basin. The sandstone body morphology in the strata is typically crescent-shaped or lenticular in shape. According to the existing lithological data of the profile or drilling, the depth range and thickness of the sandstone mass in the formation are determined. For the seismic cross-section area without drilling, the thickness of the sandstone is estimated to account for the corresponding mass. Take Jiulongjiang Sag as an example, the thickness of the sandstone body in the Taixi Basin occupies 20% to 50% of the total thickness of the layer (Wei et al., 2018). In the profile, the upper and lower boundary curves of the sandstone mass are digitized to obtain their geometry. To calculate the area of the sandstone body in the profile for each stratum, we apply the 3D geological model of the mothballed strata so that it can be applied to the stratigraphy and actual areas of the candidate caprock and reservoir rocks.

2.2. Individual reservoir resources assessment

To assess the CO_2 storage potential for individual reservoir, there have been several assessment methods, such as the US Department of Energy (US-DOE) (U.S. Department of Energy, 2007, 2008, 2010; Litynski et al., 2010), the International Geological Seal Leaders Forum for Preventing Climate Change (CSLF) (Carbon Sequestration Leadership Forum, 2005, 2007; Carbon Sequestration Leadership Forum (CSLF), 2008; Bachu et al., 2007; Bradshaw et al., 2007), the International Energy Agency Greenhouse Gas Research and Development Program (IEAGHG) (International Energy Agency Greenhouse Gas Programme, 2009; Gorecki et al., 2009), the US Geological Survey

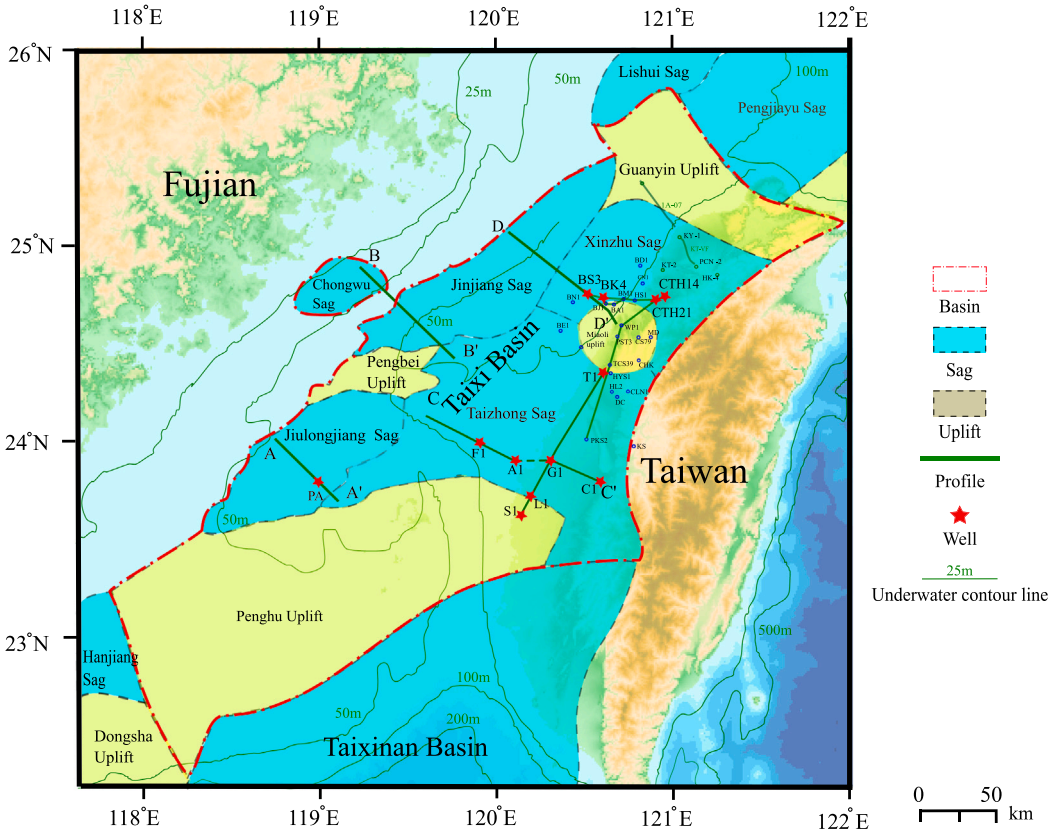

Fig. 1. Geological map of the Taixi Basin (Modified from Fu et al., 2012). The five tectonic sag units are circled in blue dashed lines. The seismic profiles are shown in green straight lines, and the red stars represent drilling wells, which are detailed in Table 1.

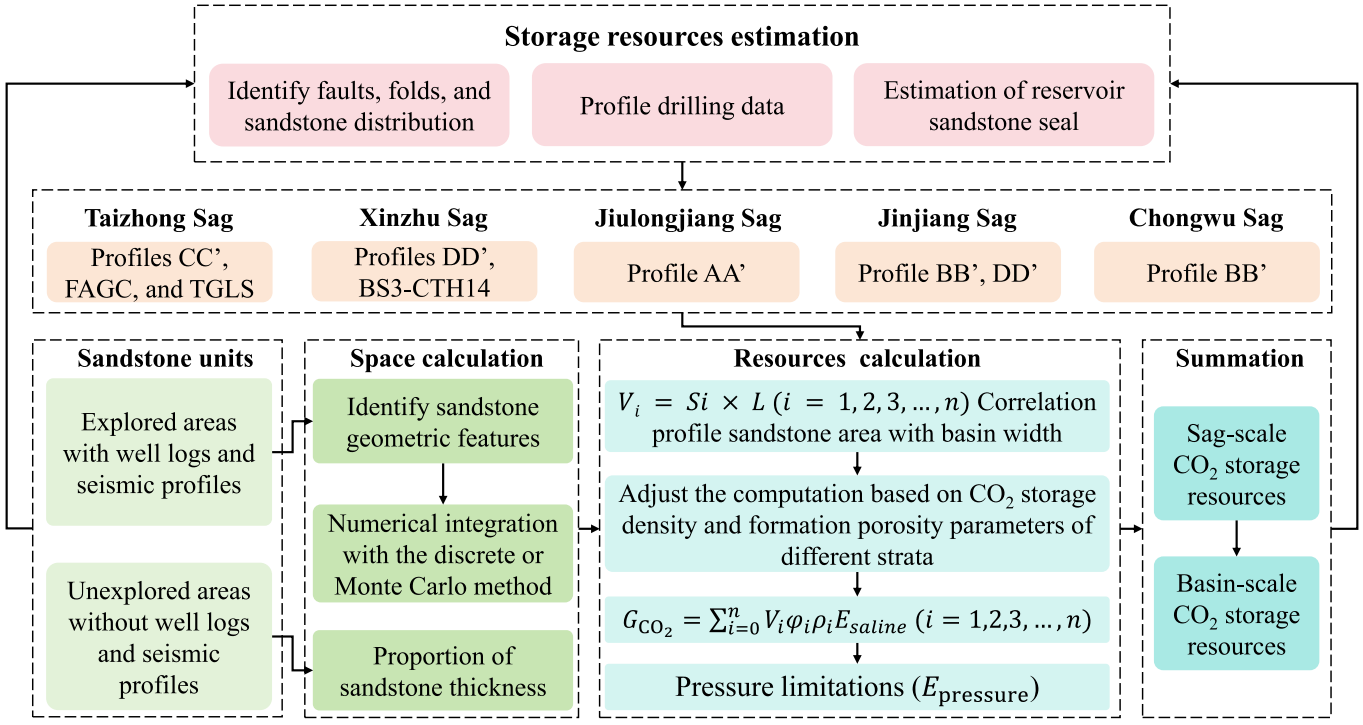

Fig. 2. The process of storage resources estimation for Taixi Basin in sag-scale.

Table 1
Seismic profiles and well logs used for analysis, where Fm. and Ss. represent Formation and Sandstone, respectively.

Type	Name	Location	Key geological information	Sag	Diagram
Seismic	AA' (Fu et al., 2012)	24.04°N, 118.91°E; 23.70°N, 119.24°E	Strata deepen from west to east and then shallower	Jiulongjiang	Figs. 1&9a
	BB' (Wei et al., 2018)	24.49°N, 119.53°E; 25.19°N, 120.14°E	A double half-graben structure deepens and becomes shallower from west to east	Jinjiang, Chongwu	Figs. 1&10a
	CC' (Lin et al., 2003)	24.20°N, 119.73°E; 23.82°N, 120.45°E	West to east, the strata deepens and then becomes shallower	Taizhong	Figs. 1&7a
	DD' (Lin et al., 2003)	24.68°N, 120.34°E; 24.69°N, 120.71°E	East to west, sedimentary thickness and sandstone content changed	Jinjiang, Xinzhu	Figs. 1&8a
	TGLS (Cai, 2016)	23.95°N, 119.91°E; 23.57°N, 120.15°E	South to north, the strata tilt northward	Taizhong	Fig. 1
	FAGC (Cai, 2016)	23.74°N, 120.60°E; 24.33°N, 120.61°E	West to east, mainly distributes below the Nanzhuang Formation	Taizhong	Fig. 1
	BS3-CTH14(Chiang, 2007)	24.74°N, 120.53°E; 24.72°N, 120.96°E	Northwest Xinzhu, reflecting changes of sag thickness and basement	Xinzhu	Fig. 1
	KTVF (Qiu, 2009)	25.04°N, 121.05°E; 24.89°N, 121.14°E	Northwest Xinzhu, reflecting changes of sag thickness and basement	Xinzhu	Fig. 1
	IA-07 (Qiu, 2009)	25.33°N, 120.83°E; 25.10°N, 121.02°E	Northwest Xinzhu, connect Xinzhu Sag and Guanyin Uplift	Xinzhu	Fig. 1
Well	PA (Zhang et al., 2019b)	On AA'	Fm. depth: 1036 to 4091.5 m	Jiulongjiang	Figs. 1&5
	T1 (Cai, 2016)	On TGLS	Fm. depth: 2749 m and 3125 m	Taizhong	Fig. 1
	G1 (Cai, 2016)	On TGLS	Fm. depth: 1918 m and 1990 m	Taizhong	Fig. 1
	L1 (Cai, 2016)	On TGLS	Fm. depth: 1152 m to 1389 m	Taizhong	Fig. 1
	S1 (Cai, 2016)	On TGLS	Fm. depth: 1066 m to 1109 m	Taizhong	Fig. 1
	F1 (Cai, 2016)	On FAGC	Fm. depth: 1598 m	Taizhong	Fig. 1
	A1 (Cai, 2016)	On FAGC	Fm. depth: 2234 m	Taizhong	Fig. 1
	C1 (Cai, 2016)	On FAGC	Fm. depth: 4709 m	Taizhong	Fig. 1
	BS3 (Chiang, 2007)	On BS3-CTH14	at junction of Shilifen & Yutengping sections	Xinzhu	Fig. 1
	BK4 (Chiang, 2007)	On BS3-CTH14	at junction of Shilifen & Yutengping sections	Xinzhu	Fig. 1
	CTH21 (Chiang, 2007)	On BS3-CTH14	Shanguji Ss. reaches 2200 m	Xinzhu	Fig. 1
	CTH14 (Chiang, 2007)	On BS3-CTH14	Shanguji Ss. exceeds 2850 m	Xinzhu	Fig. 1

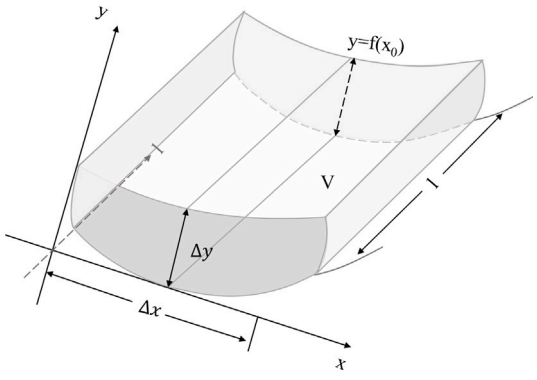

Fig. 3. A simplified model to estimate volumes of the sandstone. Δx represents the horizontal distance of the unit sandstone on the cross-section of the 2D profile, Δy represents the longitudinal thickness of the unit sandstone over the profile cross-section, and l represents the length of the sandstone extending in the sag perpendicular to the profile.

(USGS) (Blondes et al., 2013; Brennan et al., 2010), International Energy Agency/Energy and Environmental Research Center (IEA/EERC), Carbon Geological Storage Site (CGSS) and CO_2 Geocapacity (Vangkilde-Pedersen et al., 2009; Zhou et al., 2008a; Szulczewski et al., 2012). In these methods, common parameters are typically first involved, such as reservoir volume, formation porosity, supercritical carbon dioxide fluid density properties, formation storage efficiency, etc. Then, multiplication is applied to estimate the CO_2 storage resources.

Goodman et al. (2013) compared the US-DOE and CSLF methodologies and reported that US-DOE typically yields more conservative resource estimates. They emphasized that actual storage potential may vary significantly due to site-specific geological constraints. Currently, no standardized classification procedure exists for categorizing CO_2 storage estimates derived from specific assessment methodologies. The CSLF presented a Techno-Economic Resource Pyramid where CO_2 storage can be categorized into theoretical, effective, practical, and matched resources (Bachu et al., 2007). The US-DOE applies a CO_2 Storage Classification Framework analogous to the exploration and development of oil and gas accumulations. In this case, CO_2 storage can be categorized as prospective or contingent storage resources (U.S. Department of Energy, National Energy Technology Laboratory, 2010). While the CSLF Task Force and IEA-GHG (IEA Greenhouse Gas R&D Programme (IEA-GHG), 2009) reported the CSLF and US-DOE methodologies to be equivalent, the US-DOE method circumvents the heavy reliance on complex high-precision reservoir modeling inherent to the CSLF framework, thus meeting this study's requirement for efficient assessment. The US-DOE method assumes that the injection of CO_2 occupies the space previously occupied by the salt-containing aquifer and introduces a storage efficiency coefficient (E).

In this paper, we apply the US-DOE method to calculate the storage resources of each identified reservoir as:

$$G_{CO_2} = \sum_{i=1}^{n}(V_i \cdot \varphi_i \cdot \rho_i \cdot E_{saline}) \quad (i = 1, 2, 3, \ldots, n) \tag{1}$$

$$V_i = S_i \times L \tag{2}$$

where G is the CO_2 geological storage potential [t], V_i is the ith calculating unit sandstone volume [km^3], ϕ_i is the ith calculating unit sandstone porosity [%], ρ_i is the ith calculating unit carbon dioxide density under the storage conditions [kg/m^3], S_i is the ith calculating

Table 2
Parameter ranges and validity conditions (Doughty et al., 2008; Jiao, 2014).

Parameter	Sign	Calculation range	Valid values
CO_2 Density	ρ_i	250 ~ 800 kg/m^3	Pressure–temperature regression curve
Porosity	ϕ_i	17.1 ~ 37.1%	Deep regression curve
Pressure	P	150 ~ 250 bar	10 MPa/km of hydrostatic pressure gradient
Temperature	T	30 ~ 65 °C	30 °C/km of ground temperature gradient

unit sandstone area [km^2], L is the longitudinal extension distance of the formed sandstone [km], and E_{saline} is the CO_2 storage effective coefficient reflecting the ratio of the pore space volume occupied by CO_2 to the total pore volume.

The storage density of CO_2 is determined according to the formation temperature and pressure conditions ρ_{CO_2}, typically between 0.6 tons/m^3 and 0.8 tons/m^3 (Doughty et al., 2008). The specific parameter ranges are shown in Table 2. The prediction potential of CO_2 geological storage with 10%, 50%, and 90% confidence is calculated in the prefecture-level potential evaluation.

2.3. Storage efficiency factor

The storage efficiency factor (E_{saline}) is the fraction of the total pore volume within a saline formation that can be occupied by injected CO_2 (Goodman et al., 2013). It encompasses all geological or physical mechanisms that prevent the theoretical storage capacity from being fully realized. Thus, the resulting value is not a theoretical upper-bound but a practically achievable one.

The internal structure of the factor is multiplicative. Five partial efficiencies, each describing a distinct geological or displacement constraint, are multiplied together. Each successive term reduces the volume accessible to CO_2:

$$E_{saline} = E_{A_n/A_t}\, E_{h_n/h_g}\, E_{\phi_e/\phi_{tot}}\, E_V\, E_d, \tag{3}$$

where E_{A_n/A_t} is the net-to-total area ratio, which represents the portion of the basin surface underlain by formations that are sufficiently porous, permeable, and deep enough to be suitable; E_{h_n/h_g} is the net-to-gross thickness ratio, the fraction of the gross interval that actually meets the porosity and permeability criteria after excluding shale streaks, tightly cemented zones, and other non-reservoir layers; $E_{\phi_e/\phi_{tot}}$ is the effective-to-total porosity ratio, acknowledging that only interconnected pores contribute to flow, while the isolated vugs and dead-end pores do not; E_V is the volumetric displacement efficiency, a single parameter that combines areal sweep, vertical sweep, and the stabilizing or destabilizing effects of gravity, tonguing, or override; and E_d is the microscopic displacement efficiency, the proportion of the pore space that can be occupied by the injected CO_2 after accounting for irreducible water saturation (Doughty and Pruess, 2004; Koide et al., 1992; Hafeen et al., 2004; van der Meer, 1992).

In this work, the factor is treated probabilistically, represented by three percentiles that delineate the range of plausible outcomes: a conservative P_{10} of 1.2%, a median P_{50} of 2.4%, and an optimistic P_{90} of 4.1%. These values indicate, respectively, that there is only a 10% chance that the actual value will be below 1.2%, a 50% chance it will be below 2.4%, and a 90% chance it will be below 4.1% (Bachu et al., 2007), which are extracted from the distribution for clastic (sandstone) successions, using parameter ranges documented by the IEAGHG and other regional studies (IEA Greenhouse Gas R&D Programme, 2009).

2.4. Consideration of pressure limitations

While the volumetric method is suitable for regional-scale preliminary assessment, practical CO_2 storage operations will be constrained by pressure management considerations. The theoretical storage resources estimated in the previous section assume that pressure build-up during injection remains below the fracture gradient of the caprock formations. In closed or semi-closed systems, the ultimate constraint on storage resources is the pressure space that the reservoir can safely accommodate, rather than the total pore volume. Following the SPE CO_2 Storage Resources Management System (SRMS) (Society of Petroleum Engineers, 2017), our estimates represent prospective storage resources that would require confirmation through dynamic simulation and pressure analysis before advancing to commercial projects. Bump and Hovorka (2024) and Chatelan et al. (2023) demonstrate that pressure-limited storage efficiency in closed aquifers can be 30%–60% lower than volumetric estimates. Similarly, Thibeau and Adler (Thibeau and Adler, 2023) emphasize that in pressure-limited stores, the storage efficiency is controlled by the pore volume liberated by pressurization, which includes both compression of the store and water outflow, thereby bridging the gap between closed and open aquifer estimates. Therefore, the effective space created by CO_2 injection could be primarily derived from the compression of both rock and formation brine within a safe pressure limit (Zhou et al., 2008b; Chatelan et al., 2023). The theoretical storage efficiency under such pressure-limited conditions ($E_{pressure}$) can be expressed as:

$$E_{pressure} = \Delta P \times C_t, \tag{4}$$

where ΔP represents the maximum allowable pressure increase and C_t denotes the total compressibility. Given the current lack of basin-wide measured data for reservoir fracture pressure and compressibility in the Taixi Basin, a direct calculation of $E_{pressure}$ is not feasible. Consequently, we adopt a conservative, pressure-constrained efficiency coefficient range based on international studies of analogous geological settings in closed/semi-closed basins. For instance, Chatelan et al. (2023) reported storage efficiencies of 0.46%–0.52% for the basal aquifer in Western Canada when considering regional pressure buildup limits. Similarly, Bump and Hovorka (2024) calculated efficiency values ranging from 0.37% to 0.81%, with a median of 0.57%, while Zhou et al. (2008b) also concluded that storage efficiencies in closed systems are typically below 1%. This adjusted range (0.37%–0.81%) is used specifically to estimate the pressure-constrained storage resources, which provide a more realistic and engineering-relevant evaluation compared to the volumetrically-derived theoretical resources.

This adjustment aims to incorporate pressure constraints as a central consideration into our resource assessment model, thereby providing more realistic and guidance-oriented results. This study's assessment of theoretical storage resources, derived from the volumetric method, is fundamentally predicated on the assumption that the injection-induced pressure buildup is meticulously managed to remain below the fracture gradient of the caprock formations. Exceeding this threshold could compromise the seal integrity and lead to the escape of stored CO_2 (Lintong et al., 2024). Furthermore, we explicitly acknowledge the risk of re-activating pre-existing faults due to increased pore pressure. Such reactivation could create new migration pathways, jeopardizing storage security. The subsequent pressure-constrained assessment is introduced precisely to provide a more realistic estimate that inherently respects these geomechanical boundaries.

3. Geological and hydrological settings

3.1. Reginal geological characteristics

3.1.1. Location and topography

The Taixi Basin exhibits substantial dimensions, extending 460 km to 600 km in length and 230 km to 260 km in width, encompassing a

total area of approximately 12×10^4 km^2 (Fu et al., 2012) (Fig. 1). The boundaries of the basin are defined by three major geological features, namely the deformation front to the east, the Guanyin Uplift to the north, and the Penghu Terrace to the south. The average water depth of the basin is 80 m (Yang et al., 2018), and the water depth of the Taichung shoal is less than 60 m (Zhang et al., 2019a). The isothickness line of the sedimentary layer in the Taixi Basin runs in a northeast-southwest direction, with the thickness increasing eastward (Chen, 2006).

The Taixi Basin is one of the most tectonically active hydrocarbon-bearing basins offshore China, shaped by the interaction of the Philippine Sea Plate and the arc-continent collision dynamics of Taiwan. The basin has evolved through orogenic loading and flexural deformation along a rifted continental margin, resulting in a complex structural framework. This includes several key features, such as Eastern Sag (e.g., the Taizhong and Xinzhu Sags), Central Uplift (i.e., the Penghu-Beigang and Miaoli Uplifts), and Western Sag (i.e., the Jiulongjiang, Jinjiang, and Chongwu Sags) (Fu et al., 2012) (Fig. 1).

3.1.2. Structural setting

The Taixi Basin's unique tectonic setting, adjacent to the plate boundary junction and within the continent-island arc transition zone, makes it particularly susceptible to collision and compressional forces (Xue et al., 2012). The western strait region exhibits numerous large-scale NE-NNE-trending faults penetrating the pre-Cenozoic basement, predominantly normal faults with limited reverse faulting. These basement-involved fault systems demonstrate extensive spatial distribution and remarkable continuity, having controlled the regional uplift-sag architecture under the extensional regime since the late Early Cretaceous. The development of both the Coastal Fault Zone and Western Strait Fault System shows direct genetic relationships with the Taixi Basin's sedimentary evolution. Seismicity analysis reveals concentrated activity along plate boundaries, where large earthquake hypocenters frequently reactivate pre-existing normal faults, as evidenced by Quaternary seismic records in the Taixi Basin Deng (2019).

3.1.3. Basin tectonic evolution and development

The Cenozoic tectonic evolution of the Taixi Basin can be divided into three main stages. The first stage, during the Paleocene–Eocene, is characterized by rifting and the development of extensional faults and basins. The second stage, during the Miocene, is marked by large-scale subsidence and sediment accumulation. The third stage, from the Late Miocene to the Quaternary, is characterized by the development of a foreland basin associated with compressional structures and bending loads (Wei et al., 2018).

Preliminary structural analyses indicate that the Taixi Basin exhibits a dual-basin architecture comprising lower fault-bounded sequences overlain by upper depression-phase strata, separated by a regional fracture unconformity surface (Ru, 1990). The Early to Middle Jurassic rift phase was characterized by concentrated subsidence in the central and eastern parts of the basin, transitioning to stable basin-wide deposition during the Late Jurassic to Early Cretaceous sag phase. This was followed by regional uplift during the Late Cretaceous, which preferentially preserved Upper Cretaceous residual strata in the western Cenozoic depocenters (Fu et al., 2012). This polyphase tectonic history laid the foundation for the Cenozoic evolution of the basin, resulting in a modern structural framework with distinct east–west zonation and north-south compartmentalization, which has significant implications for both hydrocarbon migration and CO_2 storage resources.

The Taixi Basin's internal structure is primarily characterized by a half-graben rift system (Yu and Huang, 1994), with its Mesozoic tectonic evolution divided into two principal phases comprising the rift stage during the Early to Middle Jurassic and the subsequent post-rift subsidence stage from Late Jurassic to Early Cretaceous (Guo et al., 2015b). Stratigraphic development in the basin occurred in three main phases. The first phase, from the Cretaceous to Eocene, was dominated by fluvial-lacustrine deposits in a rift-lacustrine environment. The second phase, in the Oligocene, involved uplift and erosion, marked by regional unconformities. The third phase, from the Miocene to the present, is characterized by sedimentary subsidence, with marine-terrestrial transitional facies (Li et al., 2013).

3.2. Reservoir and caprock characteristics

The Taixi Basin exhibits a complex geological structure, primarily composed of sediments from the Pliocene to the present. The basin's stratigraphy is marked by a westward transition from coarser sediments in the foreland region to finer sediments towards the Taiwan Strait, with sediment thickness ranging from over 2000 m in the western foreland to less than 100 m in the middle of the Taiwan Strait (Covey, 1986; Yu and Chou, 2001). Sandstone reservoirs with low porosity and permeability and strong diagenesis are widely distributed in each sag zone of the Taixi Basin. The sandstone reservoirs are mainly composed of sandstones deposited in deltaic, fan deltaic, littoral-shallow marine, lacustrine, and bay facies (Fu et al., 2012).

3.2.1. Central-eastern sags

Fig. 4 shows the specific stratum composition of the Central-Eastern Sags. The Taizhong Sag and Xinzhu Sag in west-central Taiwan exhibit similar features for CO_2 storage, with well-developed reservoir and caprock systems. The Late Miocene to Pleistocene strata include reservoir sandstones, such as the Shangfuchi Sandstone in the Nankang Formation and the Guandaoaoshan and Yutengping Sandstones in the Gueizhulin Formation. The Gueizhulin Formation also serves as a tectonic boundary, with overlying foreland basin strata and underlying passive continental margin strata. The Jinshui Shale is a regional caprock due to its low permeability and extensive lateral continuity. The Zhuolan and Toukeshan Formations further contribute to the regional caprock system (Lin et al., 2003).

The lithology of the Taizhong area is preliminarily divided into four types: mudstone, interbedded sand-shale, sandstone, and conglomerate (Fig. 4). The Taixi Basin features a full sedimentary sequence from the Late Miocene to the Pleistocene. The lower section is dominated by tidally-influenced shallow marine sediments in the upper Miocene Nanzhuang Formation and lower Gueizhulin Formation (Nagel et al., 2013). The Gueizhulin Formation unconformably overlays the Nanzhuang Formation and mainly consists of deltaic deposits influenced by shallow marine tides. Its southern equivalent, the lower Gutingkeng Formation, reflects deeper marine conditions.

The Gueizhulin Formation is overlain by the Jinshui Shale, a mudrock unit that can reach up to 300 m in thickness. This shale was deposited during the maximum flooding phase, with evidence of provenance from the eastern Taiwan orogen (Chang and Chi, 1983). The Zhuolan Formation, formed from late Miocene to early Pleistocene, consists of deltaic deposits that transition to fluvial systems (Chou, 1973). The Toukeshan Formation, the youngest unit, comprises coarse sandstones and conglomerates deposited in braided river and alluvial fan environments (Covey, 1986, 1984). These stratigraphic frameworks support the feasibility of secure geological CO_2 storage in the region.

3.2.2. Western sags

Fig. 5 shows the specific stratum composition of the western sags. The Eocene strata predominantly consist of shallow marine and deltaic deposits, with delta sand bodies often forming effective reservoirs and the overlying mud shales acting as caprocks (Lei et al., 2016). Seismic surveys, including the CDW-1 A well in the Jiulongjiang Sag, have revealed a thick Eocene section with good-quality source rocks, showing a wide organic maturity range (Guo et al., 2015b). These Eocene sandstones have a porosity of 5% ~ 15% and a permeability of $(2 \sim 50) \times 10^{-3}$ μm^2, with poor reservoir physical properties.

The western sags of Taixi Basin are primarily composed of interbedded sandstone, siltstone, and shale, with mudstone intercalated with

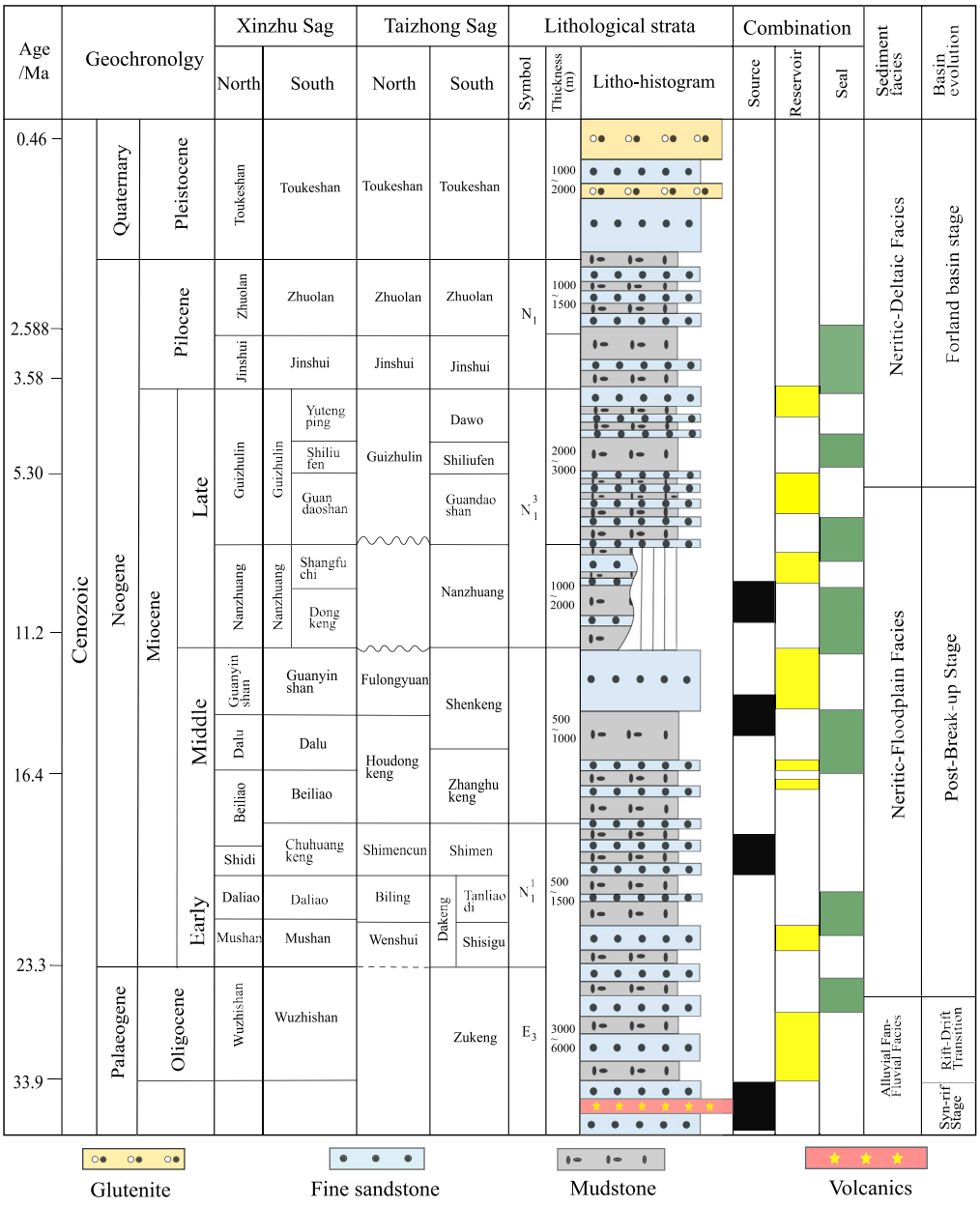

Fig. 4. Reservoir-caprock combinations in Taizhong Sag and Xinzhu Sag (Modified from (Xie and Huang, 2003)). The yellow part represents the reservoir, and the green part represents the seal.

coal seams. The Miocene has 3 sedimentary cycles, and each cycle consists of the lower littoral coal-bearing strata and the upper marine clastic strata. The specific stratum composition is shown in Fig. 5. The stratigraphic development and lithology of Jiulongjiang Sag, Jinjiang Sag, and Chongwu Sag are similar. Reservoirs are primarily developed in the Yutengping Formation, Dalu Formation, and Guizhulin Formation, where sandstones such as the Yutengping and Guandao sandstones serve as effective reservoirs (Guo et al., 2015b). Multiple hydrocarbon source rock intervals developed during these stages, primarily including the Lower Cretaceous, Paleocene, and Eocene formations (Zhang et al., 2019b).

The sandstone reservoirs in the western sags are interbedded with mudstones that serve as regional caprocks, such as the Jinshui Shale and Shiliufen Shale. Among these, the Pliocene Jinshui Shale, with a thickness of approximately 300 m, is particularly significant due to its low permeability, making it an effective caprock for CO_2 storage (Li et al., 2013). In addition to the Jinshui Shale, Lower Miocene and Eocene mudstones, as well as Neogene littoral-shallow marine mudstones, also function as excellent caprocks. These mudstones effectively seal the sandstone reservoirs in all directions, creating a secure geological configuration for CO_2 containment (Li et al., 2013). Lower Miocene, Eocene, and Neogene littoral-shallow marine mudstones also serve as effective caprocks. The Taixi Basin's source rocks, primarily in the Lower Miocene, Eocene, and Lower Cretaceous, are complemented by favorable reservoirs and caprocks, establishing three distinct reservoir-seal assemblages optimized for geological CO_2 containment. Fig. 5 shows the lithology at Well PA, which is located on Line AA' of the Jiulongjiang Sag. Oolitic sandstones were encountered in the Middle-Late Eocene strata at 2689 m (Hsiao et al., 1991a).

3.3. Geothermal characteristics

The geothermal gradients of strata offshore China exhibit significant regional variation. In stable continental shelf areas, geothermal gradients tend to be relatively low, while deeper water regions experience

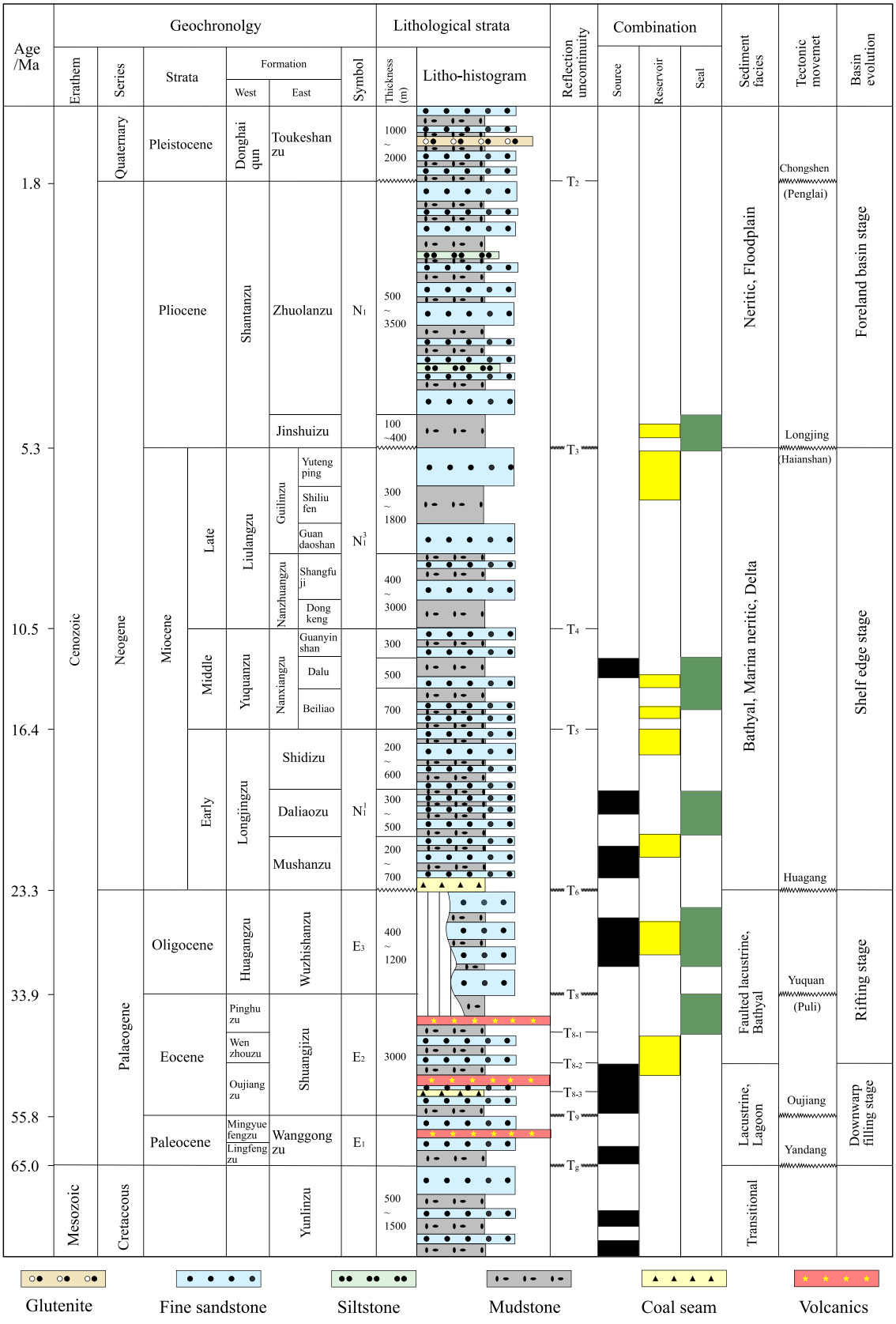

Fig. 5. Reservoir-caprock combinations in Jiulongjiang Sag at the position of well PA in Fig. 1 (Modified from (Yang et al., 2018)). The yellow part represents the reservoir, and the green part represents the seal.

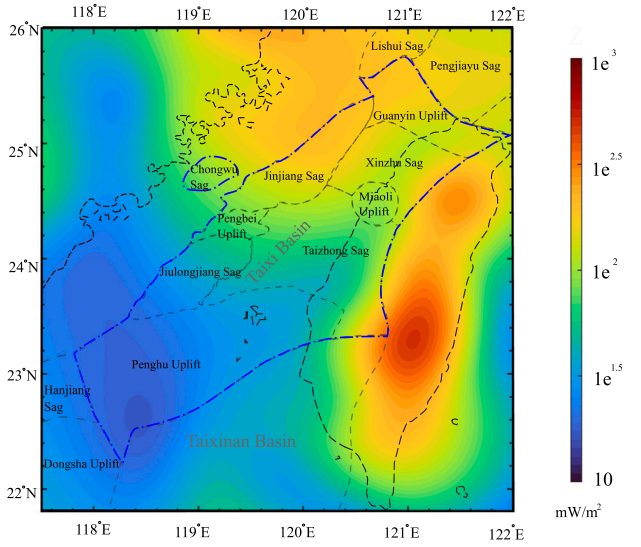

Fig. 6. Heat flow characteristics of the Taixi Basin. The color graph of a logarithmic scale is adopted to represent the *X*-axis and *Y*-axis in the heat flow intensity graph, which represent the geographical coordinates. The *Z*-axis represents the heat flow value, with the unit in logarithmic form $\log_{10}$.

higher geothermal gradients, indicating warmer basins (Qiu et al., 2020; Gong et al., 2018). In the Taixi Basin, the average geothermal temperature in the Taixi Basin ranges from 2.85 to 3 °C/100 m (Huang, 1989). However, the geothermal characteristics of different sags vary significantly, and the ground temperature near Taiwan is higher. The maximum gradient value is 5.57 °C/100 m, and the minimum gradient is 2 °C/100 m (Huang, 1989). Basins with a geothermal gradient lower than 30 °C/km can be classified as cool basins.

Heat flow, which measures the rate at which heat is transferred from the Earth's interior to the surface, provides a more accurate reflection of geothermal field characteristics than other parameters (Wu, 1991). High heat flow values are mainly concentrated in the northeastern margin of the basins, while low heat flow values are mainly concentrated in the western and southern margins (Wu, 1991). Fig. 6 shows the heat flow of the entire Taixi Basin. The geothermal gradient value in the southern margin of the basin is very high, and a small area of high heat anomaly appears in the southeastern margin. In the mature collision zone of Taiwan, the heat flow is high. The heat flow in mountainous areas mostly ranges from 80 to 250 mW/m^2 (Wei et al., 2018). According to existing data, the geothermal heat flow value of the Taixi Basin is approximately 60 mW/m^2, and the heat flow values in the Taixi Basin near the land area of Taiwan are also concentrated between 50 to 90 mW/m^2. From the perspective of the reservoir, under the condition of low heat flux (< 60 mW/m^2), the temperature is low and the CO_2 density increases, which is conducive to structural storage.

3.4. Hydrological characteristics

The process of CO_2 storage in a reservoir is influenced by various factors, such as the temperature and pressure conditions of the rock formation, and geochemistry, which are mainly related to the hydrogeological characteristics of the sedimentary basin Kang et al. (1995). Hydrogeological conditions play a critical role in determining both the resources and safety of CO_2 storage. Temperature and salinity exhibit vertically homogeneous distributions. The vertical structure of temperature and salt in this area has a stratification phenomenon. There is a strong temperature and salt cline, and the isotherm and isosaline of each section are inclined downward (Dou et al., 2010). The salinity in the Taixi Basin ranges from 29.9 to 34.4 psu (Li et al., 2014).

4. Assessment of storage potential

By combining the seismic profile and drilling data, we assess the CO_2 storage resources of each sag in Taixi Basin for CO_2 storage, by combining the seismic reflection profile data. Table 3 summarizes the storage resources assessment results for each specific formation and sag. The assessment of CO_2 storage resources integrates seismic and well data to estimate sandstone formation volumes. Significant uncertainties in these calculations arise from the following. (1) Data sparsity due to limited well and 2D seismic coverage over the vast basin area (~120,000 km^2), creating interpretation ambiguity in sandstone distribution. (2) Spatial variability in sandstone content (20%–50% net-to-gross ratio) controlled by depositional facies. (3) Simplified geological geometries when converting 2D areas to 3D volumes. These volumetric uncertainties, combined with parameter ranges in Table 2, are propagated through our probabilistic assessment. Thus, the formation volumes and resource estimates should be interpreted as model outputs with a range of possible outcomes, expressed as P_{10}, P_{50}, and P_{90} values in Table 3.

The assessment of storage potential for each sag is based on the interpretation of seismic profiles and well data. A critical criterion in our analysis has been the strategic selection of representative seismic lines and interpreted reservoir units that avoid known major fault zones with significant displacement and clear recent activity. This approach aims to identify storage complexes where the geological containment, primarily provided by the regional caprocks (e.g., Jinshui Shale), is least likely to be compromised by structural discontinuities. While this provides an optimistic view of the containment security, it is imperative to note that fault systems are pervasive in the Taixi Basin.

4.1. Taizhong Sag

The Taizhong Sag is located onshore and offshore central-western Taiwan. The subsurface strata consist of Mesozoic basement rocks and Cenozoic sedimentary layers (Fig. 4). Drilling data reveal formations including the Jinshui Shale, Guizhulin Formation, Nanzhuang Formation, Guanyinshan Sandstone, Dalu Shale, Beiliao Formation, Shidi Formation, Biling Shale, Muzhan Formation, and Wuzhishan Formation (Nagel et al., 2013). The Taizhong Sag develops three main reservoir-seal systems for CO_2 storage. The NK-C System, in which the Nanzhuang and Guizhulin Formations serve as reservoirs, is sealed by the Jinshui Shale. The thickness of the reservoir is 300–800 m, and it is eroded eastward. The SP-T System, where the Shidi and Beiliao Formations act as reservoirs, is sealed by the Dalu Shale, continuously distributed, with a thickness of 400 ~ 1200 m. The WM-P System, in which the Wuzhishan and Muzhan Formations function as reservoirs, sealed by the Biling Shale, has a burial depth of 3000 m and a stable thickness (500–1000 m) (Cai, 2016). Overall, the reservoir-seal systems in the Taixi Basin are highly favorable, providing excellent conditions for geological carbon storage. The cross-section CC' (Fig. 7a) extends from the northwest (24.20°N, 119.73°E) to the southeast (23.82°N, 120.45°E). Four holes at F1, A1, G1 and C1 were drilled on profile CC'(Fig. 1). The Nanzhuang Formation pinches out eastward and is absent in Well C1. Influenced by the tectonic loading of the orogenic belt to the east, the strata exhibit an overall eastward dip. Post-rift sequences thin towards the east, while foreland basin strata thicken in the same direction. The sandstone strata reach depths exceeding 3000 m (Fig. 7). This section covers the Oligocene-Miocene post-breakup sediments, which are then flexed downwards by the Taiwan orogen in the east (Lin et al., 2003).

Due to the loading effect of the eastern orogenic belt, the strata generally dip eastward. Post-rift strata thin eastward, while foreland basin strata thicken eastward. There are also four wells T1, G1, L1, and S1 from Northeast to Southwest (Fig. 1). From well T1 to S1, the top of the Guanyinshan Sandstone is adjusted to a horizontal reference. Post-rift strata thin southward with onlapping, and the overall strata dip

Table 3
Geological formations and CO_2 resources of the five sags in the Taixi Basin.

Sag	Formation	Volume	Porosity	Density	Theoretical resources (tons)			Effective resources (tons)		
		(km^3)	(%)	(kg/m^3)	P_{10} = 1.2%	P_{50} = 2.4%	P_{90} = 4.1%	P_{10} = 0.37%	P_{50} = 0.57%	P_{90} = 0.81%
Xinzhu	Yutengping (east)	460.152435	22–30	325–625	7.80E+08	1.56E+09	2.67E+09	2.41E+08	3.71E+08	5.27E+08
	Guandaoshan (east)	424.403679	17–25	325–625	6.95E+08	1.39E+09	2.37E+09	2.14E+08	3.30E+08	4.68E+08
	Shangfuji (east)	218.754982	15–22	325–625	3.28E+08	6.57E+08	1.12E+09	1.01E+08	1.56E+08	2.21E+08
	Western Zone	163.320987	15–28	325–625	2.45E+08	4.90E+08	8.37E+08	7.55E+07	1.16E+08	1.58E+08
	Total	1606.63	–	–	2.03E+09	4.10E+09	7.00E+09	2.35E+08	2.34E+08	1.05E+09
Taizhong	Nanzhuang	3186.16	15.7–29.4	450–630	5.01E+08	1.00E+10	1.71E+10	1.54E+09	2.38E+09	3.38E+09
	Guizhulin	1222.49	17.7-23	550–600	4.92E+08	9.84E+08	1.68E+09	1.52E+08	2.34E+08	3.32E+08
	Guanyinshan	500.825	13.3–27.55	490–630	6.57E+08	1.31E+09	2.25E+09	2.03E+08	3.11E+08	4.45E+08
	Dalu (thin)	324.526	13.3–27.55	500–630	4.53E+08	9.05E+08	1.55E+09	1.40E+08	2.15E+08	3.06E+08
	Beiliao (faulted)	211.52	8.9–25.7	500–665	3.32E+08	6.64E+08	1.13E+09	1.02E+08	1.58E+08	2.23E+08
	Shidi	258.806	19.3–23.6	500–630	3.88E+08	7.77E+08	1.33E+09	1.20E+08	1.85E+08	2.63E+08
	Mushan	984.586	17.7–20.8	600–640	1.41E+09	2.82E+09	4.82E+09	4.35E+08	6.70E+08	9.52E+08
	Wuzhislam	509.117	16.7–23.4	550–640	7.12E+08	1.42E+09	2.48E+09	2.20E+08	3.37E+08	4.80E+08
	Total	7198.02	–	–	9.45E+09	1.89E+10	3.88E+10	2.19E+09	4.49E+09	7.67E+09
Jiulongjiang	Middle Eocene	547.87	18–28	470–707	7.90E+08	1.58E+09	2.78E+09	2.44E+08	3.75E+08	5.33E+08
	Lower Eocene	491.83	18–29	470–707	7.09E+08	1.42E+09	2.42E+09	2.19E+08	3.37E+08	4.78E+08
	Palecocene	121.59	18–30	470–707	1.75E+08	3.51E+08	5.99E+08	5.40E+07	8.34E+07	1.18E+08
	Total	1161.28	–	–	1.67E+09	3.35E+09	5.72E+09	5.15E+08	7.96E+08	1.13E+09
Jinjiang	Sand-Mudstone	1950.39	18–28	500–707	2.81E+09	5.63E+09	9.61E+09	8.66E+08	1.34E+09	1.90E+09
Chongwu	Sand-Mudstone	217.535	18–28	500–707	3.14E+08	6.27E+08	1.07E+09	9.68E+07	1.49E+08	2.11E+08
Total			–	–	1.63E+10	3.26E+10	6.22E+10	5.03E+09	7.74E+09	1.23E+10

northward. The Nanzhuang Formation pinches out in the southern section, while the foreland basin sequence, which contains the Guizhulin Formation to the lower Toukeshan Formation, is absent in Wells F1 and S1 (Cai, 2016). Therefore, stratigraphic variations must be carefully considered when estimating storage resources.

Based on the sandstone thicknesses of different formations in four boreholes along the east–west CC' cross-section and the distances between boreholes, the areas of formation sandstones in the 2D cross-section can be determined. The strata exhibit uplift east of Well G1, with formations below the Dalu Group absent east of this borehole. Sandstones are continuously distributed from the Jinshui to Wuzhishan formations along this profile, with the Nanzhuang to Wuzhishan formations serving as primary reservoirs at depths of 500 ~4000 m. Formation depths progressively increase from Well F1 eastward to Well C1. A significant uplift occurs south of Well G1 along the north-south direction, with thicker sandstone accumulations observed at the northernmost Well T. Sandstones exist within the Jinshui Shale to Dalu Group interval, with thicknesses ranging from 2430 m ~ 3760 m. The Mushan and Wuzhishan layers are present between boreholes G1–L1 and L1–S1. The Nanzhuang Formation sandstone with a volume of 3186 km^3 possesses a theoretical resources of 10 Gt and effective resources of 2.38 Gt, while the Guizhulin Formation of 392 km^3 possesses 0.98 Gt theoretical resources and 0.23 Gt effective resources. The Guanyinshan Formation exhibits 501 km^3 sandstone volume and 1.31 Gt storage theoretical resources, and the Dalu Group's 324 km^3 sandstone volume provides 0.9 Gt theoretical resources. The thinner Beiliao and Shidi formations offer respective theoretical resources of 0.66 Gt and 0.78 Gt. The Mushan Formation contains 984 km^3 sandstone with 2.82 Gt theoretical resources, and the Wuzhishan Formation's total sandstone volume of 509 km^3 yields 1.42 Gt theoretical resources. The effective resources are about 23.75% to 50.6% of the theoretical resources. The Nanzhuang Formation demonstrates exceptional potential as the most effective reservoir stratum (Table 3). The total theoretical storage resources of Taizhong Sag are 18.9 Gt, and the effective resources are 4.49 Gt.

4.2. Xinzhu Sag

The Xinzhu Sag is in the northwestern region of Taiwan. The Taiwan Foreland Basin developed along the passive continental margin Teng (1990). To the north of the Taipei High, the complete stratigraphic sequence comprises the Late Miocene Guizhulian Formation, the Pliocene Jinshui Shale, the Zhuolan Formation, and the Pleistocene Toukoushan Formation (Teng, 1990; Chiao et al., 2011) (Fig. 4). The Xinzhu Sag is in the northwestern region of Taiwan, with sediments thickening from west to east. The thickness of sandstone increases towards the east. The maximum sedimentary thickness in the Xinzhu Sag reaches up to 8000 m. Fig. 8 shows a 3D reservoir cap formation, where the strata below the caprock can be used as reservoirs exceed 3000 m.

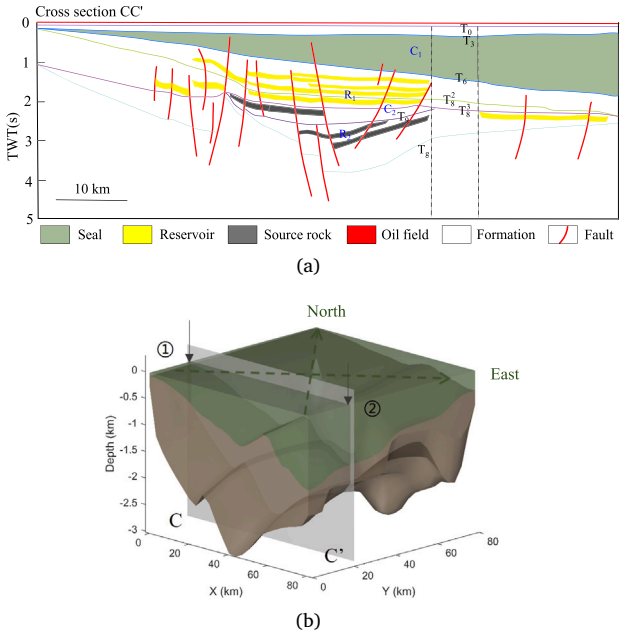

Fig. 7. Taizhong Sag (Lin et al., 2003) **(a)** 2D geological cross-section CC'; **(b)** 3D visualization of Taizhong Sag, with the green region representing the area from sea level to the top of the seal, and the brown region indicating the area below the capstone. ① 24.20° N, 119.73° E ② 23.82° N, 120.45° E. The symbol R represents reservoirs, and the symbol C represents caprocks.

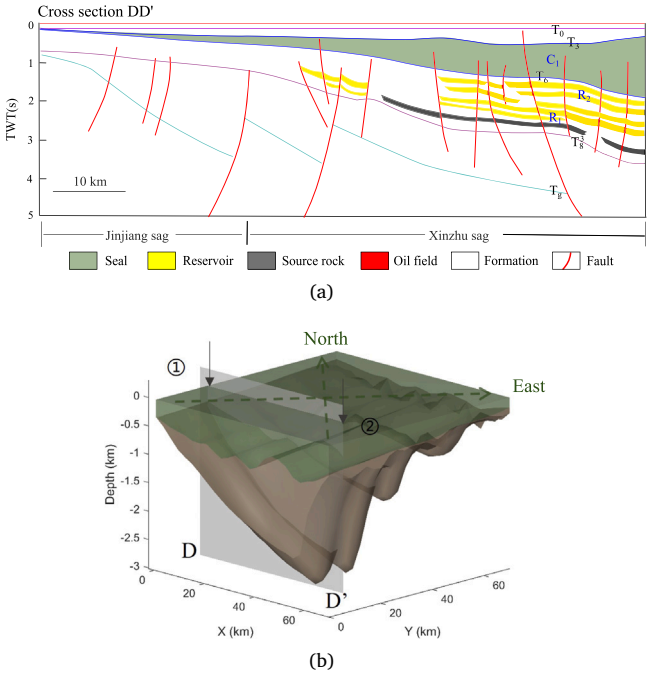

Fig. 8. Xinzhu Sag (Lin et al., 2003) **(a)** 2D geological cross-section DD'; **(b)** 3D visualization of Xinzhu Sag, with the green region representing the area from sea level to the top of the seal, and the brown region indicating the area below the capstone. ① 24.68°N, 120.34°E ② 24.69°N, 120.71°E.

The cross-section DD' starts from the Jinjiang Sag in the west and passes through the Xinzhu Sag in the east. The profile DD' (Fig. 8a) extends from the west (24.68°N, 120.34°E) to the east (24.69°N, 120.71°E). The sedimentary sequence thickens eastward, increasing from less than 1000 m to over 2500 m, accompanied by a concurrent rise in the proportion of sandstone. The sediments in the Xinzhu Sag gradually thicken from west to east, and the thickness of the sandstone increases. The Sag also includes an E-W trending northern section BS3-CTH14 incorporating well data from eight boreholes, which are BS3, BK4, BJ3, BA1, BM1, HS1, CTH21, and CTH14 (Fig. 1). In this profile, the Guandaoshan Sandstone Member shows no significant thickness variation along the E-W direction, while the Yutengping Sandstone Member exhibits marked E-W thickness changes. Additionally, shale responses in the Yutengping Sandstone Member gradually decrease in western borehole data (Chiang, 2007). The east–west profile KTVF (Fig. 1) and section 1A-07, which connects the Xinzhu Sag and the Guanyin Uplift, also show that the northwest-southeast trending basin thickness changes in the northwest area of the sag, and the basin foundation deepens from west to east (Qiu, 2009).

Based on the sandstone thickness of the BS3-CTH14 well in the west-to-east section DD of Xinzhu Sag, the distribution areas of the Yutengping sandstone, Guandaoshan sandstone, and Shangfuji sandstone between every two wells were calculated. According to the extension distance of the formation sandstone perpendicular to the drilling direction on the scale, the volume of the sandstone passing through Xinzhu Sag is about 163 km^3. The sandstone volumes of BS3-BK4, BK4-BM1, BM1-HS1, HS1-CTH21 and CTH21-CTH14 are 199 km^3, 280 km^3, 133 km^3, 386 km^3 and 104 km^3, respectively, with a total volume of 1,267 km^3 (Table 3). The estimation results show that the total theoretical storage resources of Xinzhu Sag are 4.10 Gt, and the effective resources are 0.23 Gt.

4.3. Jiulongjiang Sag

The Jiulongjiang Sag is in the southwest Taixi Basin, with an area of about 4500 km^2 (Lei et al., 2016) with seven unconformities developed. The results show that the Jiulongjiang Sag experienced the middle and late Eocene and the middle and late Miocene phase II volcanic activity, which has a certain role in promoting the maturity of the source rocks in the area (Huang et al., 2024). The proportion of thick sandstone is relatively high, the shallow cover is relatively thin, and the strata tend upward towards the land Huang et al. (2024).

Northwestern flank of the Jiulongjiang Sag experienced significant uplift-induced stratal erosion, with a maximum denudation thickness of 770 m. In contrast, continuous subsidence persisted in the southeastern flank. Fig. 9a shows the terrain-based cross-section AA' in the Jiulongjiang Sag, which reveals the location of sandstone and source rock. The cross-section AA' extends from the northwest (24.04°N, 118.91°E) to the southeast (23.70°N, 119.24°E). The stratigraphic thickness reaches its maximum at the center of the Sag and thins significantly towards the northwest due to uplift and erosion, with a maximum eroded thickness of 770 m (Wei et al., 2018). Towards the southeast, it gradually transitions into a zone of continuous subsidence. The 3D model (Fig. 7b) reveals that the reservoir (brown area) underlying the cap rock (green area) exhibits an asymmetrical half-graben structure, characterized by a steeply dipping northwestern flank and a gently dipping southeastern flank. The sandstone bodies are primarily distributed within the central subsidence zone and along the southeastern slope. The burial depth of the sandstone strata exceeds 4000 m at its deepest point. Oligocene sandstones with partial and loose cementation constitute favorable oil and gas reservoirs, where hydrocarbons have been discovered. The Miocene succession, divided into three sedimentary cycles and corresponding stratigraphic units from base to top, forms Taiwan's three major coal-bearing strata and oil and gas reservoirs.

The area of sandstone in the Oligocene and Eocene strata passed through the AA' section of the Jiulongjiang Sag is 8.5 km^2, and the area of sandstone in the Paleocene strata is 1.3 km^2. According to (2), the volume of sandstone that AA' past from west to east was calculated and extends to the entire basin. It was obtained that the volume of sandstone in this area is 1,161 km^3 (Table 3). The estimation results show that the total storage theoretical resources of Paleocene, Eocene, and Miocene strata of Jiulongjiang Sag are 3.35 Gt, and the effective resources are 0.796 Gt.

4.4. Jinjiang Sag

The Jinjiang Sag possesses fault-block sag structures characterized by eastward normal faulting and westward overthrusting. It is manifested as the NE-SW extension differentiation. The Paleocene distribution is stable, with a relatively significant burial depth (Fu et al., 2012). The development of the biogenic reservoir-caprock combination in the Jinjiang Sag occurred during the Cretaceous to Paleocene periods (Li et al., 2007).

Fig. 10 shows the cross-section profile BB' with a length of 79 km, and the northwest end begins in the Chongwu Sag and enters the Jinjiang Sag in the southeast. The profile BB' shows that the central part is convex and the two ends are in a semi-graben shape. The BB' cross-section (Fig. 10a) extends from the northwest (24.49°N, 119.53°E) to the southeast (25.19°N, 120.14°E). The Sag exhibits a double half-graben structure. The northwestern segment is controlled by an NWW-trending normal fault, with strata dipping southeastward. The southeastern segment is influenced by a NE-trending listric normal fault, with strata dipping northwestward. The 3D model (Fig. 10b) reveals a greater fault displacement at the southeastern end, where stratigraphic thickness increases significantly. The sandstone subsidence center reaches depths exceeding 4000 m, and intrusive bodies are present along the margins. The reservoir, composed of interbedded

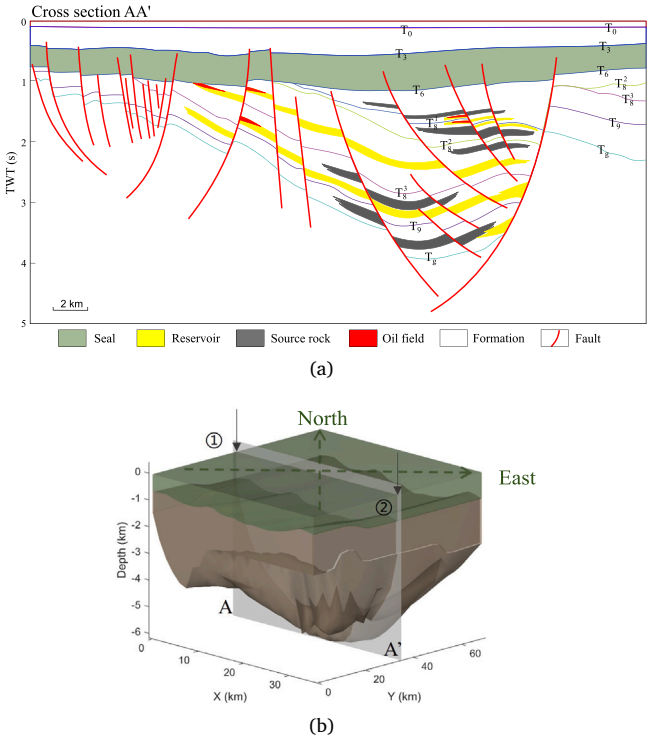

Fig. 9. Jiulongjiang Sag. **(a)** 2D geological cross-section AA'; **(b)** 3D visualization of Jiulongjiang Sag, with the green region representing the area from sea level to the top of the seal, and the brown region indicating the area below the capstone. The latitude and longitude coordinates of AA' are labeled. ① 24.04°N, 118.91°E ② 23.70°N, 119.24°E. The gray-green layer shows the position of the seal. Faults may provide additional migration channels for CO_2, causing it to escape from the storage layer.

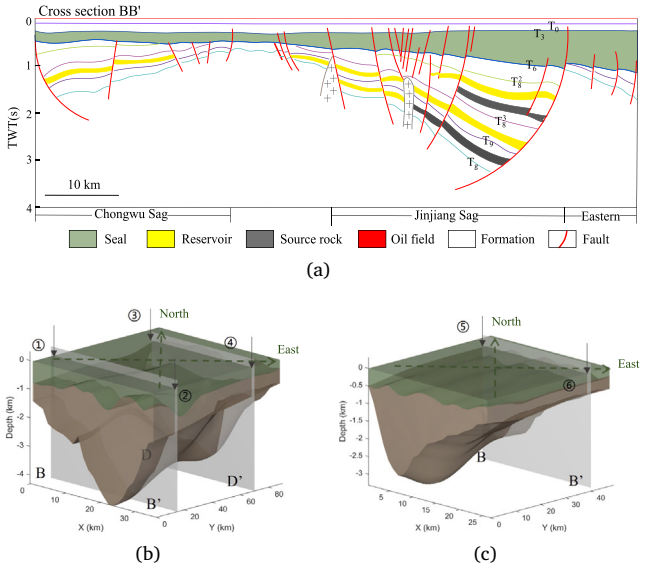

Fig. 10. Jinjiang Sag and Chongwu Sag. **(a)** 2D geological cross-section BB'; **(b)** 3D visualization of Jinjiang Sag, with the green region representing the area from sea level to the top of the seal, and the brown region indicating the area below the capstone. ① 24.49°N, 119.53°E ② 25.19°N, 120.14°E ③ 25.07°N, 120.08°E ④ 24.88°N, 120.40°E; **(c)** 3D visualization of Chongwu Sag. ⑤ 24.99°N, 119.36°E ⑥ 24.85°N, 119.46°E.

sandstone and mudstone, is distributed in a banded pattern along the fault zones, with the maximum continuous thickness located along the axial zone of the depression. Both semi-graben margins have positive and reverse normal faults. The thickness of the semi-graben strata at the southeast end is relatively large, the fault distance of the main fault is large, and there is rock mass intrusion at the edge of the semi-graben (Wei et al., 2018).

The BB' section of Jinjiang Sag passes through part of the Oligocene and Eocene sandstones, with an area of 11 km^2 and 3 km^2 of Paleocene sandstones. When calculating storage resources, the sandstone of the corresponding strata of BB' and DD' from west to east needs to be considered. The whole area includes the area south of BB', the area south of DD', north of BB', and the area north of DD', where Jinjiang sag is uplifted at DD'. The total storage volume is 1950 km^3 (Table 3). The estimation results show that the total storage theoretical resources of Jinjiang Sag are 5.63 Gt, and the effective resources are 1.34 Gt.

4.5. Chongwu Sag

The Chongwu Sag is a Neogene half-graben, which exhibits potential for CO_2 storage within its multi-layered siliciclastic succession. The Chongwu Sag is controlled by the NW-direction faults (Fig. 8c), and BB' in Chongwu is from (24.99°N, 119.36°E) to (24.85°N, 119.46°E). The strata exhibit a typical half-graben structure, with westward-dipping layers resulting from fault-controlled subsidence on the eastern side. Although no well data are available, seismic interpretation indicates that the Eocene lacustrine mudstone (caprock) and the Miocene littoral sandstone (reservoir) together form a westward-thinning wedge. The reservoir thickness decreases towards the basin margin, tapering to less than 500 m. Geophysical surveys reveal over 2000 m of Cenozoic sediments, comprising Eocene-Oligocene lacustrine mudstones (potential caprock) and Miocene-Pliocene coastal sandstones (primary reservoirs), with structural closure enhanced by NNE-striking boundary faults (China Geological Survey, 2018; Liu et al., 2020). Stratigraphic correlations suggest analogous sealing efficiency to the adjacent Jinjiang Sag, where shale gouge ratios (SGR) exceed 0.6 along fault zones (Taiwan CPC Corporation, 2019). Post-rift thermal subsidence during the Neogene (Liu et al., 2020) promoted sediment compaction, reducing fracture risks compared to active margins.

The stratigraphic sandstone area of BB' through Chongwu Sag is 4.9 km^2, and the corresponding sandstone volume is 218 km^3. BB' is located in the northernmost part of the Chongwu Sag. The stratum at the center of the sag becomes deeper, and the width of the sag becomes larger. Since the profile BB' is not completely crossed in the Chongwu Sag, the estimated data result is multiplied by 1.5 as the estimation result of the Chongwu Sag, according to the sandstone development of the Jinjiang Sag in the calculation (Table 3). The estimation results show that the total storage theoretical resources of Chongwu Sag are 0.627 Gt, and the effective resources are 0.149 Gt.

5. Conclusions and discussion

This study systematically assessed the CO_2 geological storage resources of five major sags in the Taixi Basin using the DOE volumetric methods, both without and with considering the pressure limitations. The assessment was based on 3D geological modeling with multiple seismic and well input data covering the five sags. The results show that the Taixi Basin possesses 16.3–62.2 Gt of theoretical CO_2 storage resources, with an average of 32.6 Gt; and 5.03–12.3 Gt of effective resources, with an average of 7.74 Gt. Thus, this study provides a first-order screening of the Taixin Basin for CO_2 geological storage.

This study also guides future data acquisitions. The sag-scale analysis has prioritized areas with well-developed regional caprocks (e.g., the extensive Jinshui Shale) and has intentionally avoided major fault

zones in its resource calculation. However, the presence of numerous faults, particularly in the tectonically active eastern part of the basin, remains a primary concern. The integrity of these faults as potential seals or their risk of being reactivated as conduits for CO_2 migration requires rigorous, site-specific evaluation. Therefore, new wells and 3D seismic profiling should be acquired to detail fault mapping, calculate the shale gouge ratio (SGR), conduct geomechanical modeling, and assess the likelihood of fault reactivation under projected injection pressures. Similarly, for the early planning and initial site selection of offshore CO_2 geological storage projects, the areas with a dense distribution of faults presented in this work should be avoided.

5.1. Main limitations

While providing a comprehensive evaluation of the theoretical storage resources in deep saline aquifers at the regional scale of the Taixi Basin, we acknowledge that there are still several methodological simplifications. Firstly, the static assessment approach neglects dynamic processes during carbon storage, including multiphase flow migration and pressure transmission. Secondly, due to current data limitations, the efficiency coefficients used in this assessment are based on geological analogs rather than specific rock mechanics and fluid compressibility measurements from reservoirs. This could introduce uncertainties.

5.2. Recommendations for future work

For practical implementation, the next steps would be to move towards contingent storage resources under the SRMS framework. Specifically, it is essential to acquire 3D seismic profiles in key sags, add targeted new wells, and collect basic reservoir/caprock data. Moreover, extensive work would need to be done to address the co-evolution of compressibility, miscibility, and solubility throughout the storage lifecycle, and account for local constraints such as the activity of the fault zone and lithological heterogeneity corrections to the storage efficiency coefficient in basin-specific formations.

CRediT authorship contribution statement

Jianghui Li: Writing – review & editing, Supervision, Resources, Project administration, Methodology, Funding acquisition, Formal analysis, Conceptualization. **Yanni Hou:** Writing – original draft, Visualization, Software, Resources, Investigation, Formal analysis. **Fengling Yu:** Writing – review & editing, Supervision, Methodology. **Daolong Zhou:** Visualization, Software. **Hengnian Dong:** Software. **Xiaokang Zhang:** Resources.

Declaration of competing interest

The authors declare that they have no known competing financial interests or personal relationships that could have appeared to influence the work reported in this paper.

Acknowledgments

Thanks to the National Major Science and Technology Projects of China (No. 2024ZD1406600, 2024ZD1406604, 2024ZD1406604-11), the Natural Science Foundation of Xiamen Municipality (No. 3502Z202373006), and the MEL Internal Program (No. MELRI2303) for supporting this research financially.

Data availability

The data that has been used is confidential.

References

Taiwan Environmental Protection Administration, 2023. 2023 Greenhouse Gas Inventory Report. Taipei, China.
Fujian Bureau of Statistics, 2023. Fujian Energy Statistical Yearbook 2023. Fuzhou, China.
Bachu, S., Bonijoly, D., Bradshaw, J., Burruss, R., Holloway, S., Christensen, N.P., Mathiassen, O.M., 2007. CO_2 storage capacity estimation: Methodology and gaps. Int. J. Greenh. Gas. Con. 1 (4), 430–443.
Bachu, S., Shaw, J., 2003. Evaluation of the CO_2 sequestration capacity in Alberta's oil and gas reservoirs at depletion and the effect of underlying aquifers. J. Can. Pet. Technol. 42 (9), 51–61.
Blondes, M., Brennan, S., Merrill, M., Buursink, M., Warwick, P., Cahan, S., Corum, M., Cook, T., 2013. National assessment of geologic carbon dioxide storage resources. U.S. Geol. Surv. Circ. 1386.
Bradshaw, J., Bachu, S., Bonijoly, D., Burruss, R., Holloway, S., Christensen, N., Mathiassen, O., 2007. CO_2 storage capacity estimation: Issues and development of standards. Int. J. Greenh. Gas. Con. 1, 62–68.
Brennan, S., Burruss, R., Merrill, M., Freeman, P., Ruppert, L., 2010. A methodology to estimate the CO_2 storage capacity of fractured reservoirs. Energy Procedia 4, 4818–4825.
Bump, A.P., Hovorka, S.D., 2024. Pressure space: The key subsurface commodity for CCS. Int. J. Greenh. Gas. Con. 136, 104174.
Cai, M., 2016. Assessment of geological CO_2 sequestration system in the Taihsi Basin, onshore and offshore central Taiwan. In Chinese.
Cao, M., Chen, J., 2022. The site selection geological evaluation of the CO_2 storage of the deep saline aquifer. Acta Geol. Sin. 96 (5), 1868.
Carbon Sequestration Leadership Forum, 2005. Estimation of CO_2 Storage Capacity in Geological Media. Technical Report, CSLF.
Carbon Sequestration Leadership Forum, 2007. Comparison Between Methodologies for CO_2 Storage Capacity Estimation. Technical Report, CSLF.
Carbon Sequestration Leadership Forum (CSLF), 2008. Comparison between methodologies recommended for estimation of CO_2 storage capacity in geological media. In: Bachu, S. (Ed.), Carbon Sequestration Leadership Forum (CSLF). pp. 1–15, In: Bachu, S. (Ed.).
Chang, S., Chi, W., 1983. Neogene nannoplankton biostratigraphy in Taiwan and the tectonic implications. Pet. Geol. Taiwan 19, 93–147.
Chatelan, L., Thibeau, S., Frailey, S., 2023. Application of the storage resources management system to a regional open aquifer using a notional project. Int. J. Greenh. Gas. Con. 129, 103959.
Chen, M., 2006. Sediment Velocity Structures in the Taiwan Strait and the Coastal Plain of West Taiwan. Master's thesis. National Central University, Taiwan, In Chinese with English abstract.
Chen, J., Li, X., Wang, Q., 2024. Basin-scale evaluation of CO_2 storage potential in China's offshore sedimentary basins. Mar. Pet. Geol. 158, 106582.
Chiang, S., 2007. Early development of the central Taiwan Foreland Basin revealed from stratigraphic record. In: Proceedings of the Taiwan Geological Society Annual Meeting. Stratigraphic record of the early foreland basin in central Taiwan.
Chiao, C., Lin, J., Yu, C., Lu, C., 2011. Study of late miocene to pleistocene sedimentary strata in the Southern Taixi basin as a geological carbon sequestration reservoir. Min. Met. 55 (1), 109–128.
China Geological Survey, 2018. Hydrocarbon Resource Evaluation of the Western Taiwan Strait Basins. Technical Report, (GHSC-2018-022), Ministry of Natural Resources, China.
Chou, J., 1973. Sedimentology and paleogeography of the upper cenozoic system of western Taiwan. Proc. Geol. Soc. China 16, 111–143.
Covey, M., 1984. Sedimentary and Tectonic Evolution of the Western Taiwan Foredeep (Ph.D. thesis). Stanford University.
Covey, M., 1986. The evolution of foreland basins to steady-state: Evidence from the western Taiwan foreland basin. In: Allen, P.A., Homewood, P. (Eds.), Foreland Basins. In: International Association of Sedimentologists Special Publication, vol. 8, Blackwell Scientific Publications, pp. 77–90.
Deng, K., 2019. Tectonic characteristics of the Binhai Fault zone in Taiwan strait. Mar. Geol. Quat. Geol. 39 (6), 72–80.
Diao, Y., Ma, X., Li, X., Zhang, C., Liu, T., 2021. Evaluation methods of underground space utilization for CO_2 geological storage in deep saline aquifers. Geol. Surv. China 8, 87–91.
Dou, W., Liu, X., Wang, T., 2010. The origin of formation water and the regularity of gas and water distribution for the sulige gas field Ordos basin. Acta Pet. Sin. 31, 767–773.
Doughty, C., Freifeld, B., Trautz, R., 2008. Site characterization for CO_2 geologic storage and vice versa: The Frio Brine Pilot, Texas, USA as a case study. Environ. Geol. 54 (8), 1635–1656.
Doughty, C., Pruess, K., 2004. Modeling supercritical carbon dioxide injection in heterogeneous porous media. Vadose Zone J. 3, 837–847.
Fu, Z., Jiang, X., Wang, H., Wang, G., 2012. Geological features and hydrocarbon prospect of the western depression, Taixi Basin. Mar. Geol. Front. 28 (7), 30–35.
Gong, J., Yang, C., Li, G., 2018. Geothermal gradient and heat flow distribution on the northern slope of the south China sea. In: Progress in Marine Geophysical Survey in China. Science Press, pp. 156–170.

Goodman, A., Bromhal, G., Strazisar, B., Rodosta, T., Guthrie, W.F., Allen, D., Guthrie, G., 2013. Comparison of methods for geologic storage of carbon dioxide in saline formations. Int. J. Greenh. Gas. Con. 18, 329–342.
Gorecki, C., Sorensen, J., Bremer, J., Knudsen, D., Holubnyak, Y., Smith, S., Ayash, S., Steadman, E., Harju, J., 2009. Development of storage coefficients for carbon dioxide storage in deep saline formations. Energy Procedia 1, 3119–3126.
Guo, J., Wen, D., Zhang, S., Xu, T., Li, X., Diao, Y., Jia, X., 2015a. Potential and suitability evaluation of CO_2 geological storage in major sedimentary basins of China, and the demonstration project in Ordos Basin. Acta Geol. Sin. (English Edition) 89, 1319–1332.
Guo, J., Wen, D., Zhang, S., et al., 2015b. Evaluation of CO_2 geological storage potential and demonstration projects in China. Geol. Surv. China 2 (4), 36–46.
Guo, J., Zhang, S., Diao, Y., Li, X., Fan, J., 2011. Site selection method of CO_2 geological storage in deep saline aquifers. J. Jilin Univ. (Earth Sci. Edition) 41, 1084–1091.
Hafeen, A., Croiset, E., Douglas, P.L., Chatzis, I., 2004. CO_2 sequestration in Ontario, Canada. Part 1: storage evaluation of potential reservoirs. Energy Convers. Manage. 45, 2645–2659.
Hsiao, P., Hu, C., Lin, K., et al., 1991a. Assessment of hydrocarbon potential in Penghu basin. Pet. Geol. Taiwan 26, 215–229, In Chinese.
Hsiao, P., et al., 1991b. Assessment of hydrocarbon potential in the Penghu Basin. Taiwan Pet. Geol. 26, 44–47, In Chinese with English abstract.
Huang, R., 1989. Characteristics of temperature and salinity in the central and northern Taiwan strait. Mar. Sci. (6).
Huang, C., Lin, J., Peng, Y., Chen, C., Tsao, T., Shiao, T., 2024. Offshore Taiwan: A prospective 'oasis' for geological carbon storage.
Huo, C., 2014. Assessment of carbon sequestration capacity in China's continental shelf basins. Acta Geol. Sin. (English Edition) 88 (3), 921–934.
IEA Greenhouse Gas R&D Programme, 2009. Development of Storage Coefficients for CO_2 Storage in Deep Saline Formations. Report, (2009/13), International Energy Greenhouse Gas R&D Programme.
IEA Greenhouse Gas R&D Programme (IEA-GHG), 2009. Development of Storage Coefficients for CO_2 Storage in Deep Saline Formations. Report, (2009/13), IEA Greenhouse Gas R&D Programme.
International Energy Agency Greenhouse Gas Programme, 2009. CO_2 Storage Capacity Estimation Methodology. Technical Report, (2009/02), IEAGHG.
Jiang, H., Shen, P., Song, X., 2008. Global warming and current status and prospect of CO_2 underground storage. J. Palaeogeogr. 10 (3), 323–328.
Jiao, Z., 2014. Assessment of Effective Storage Capacity and Safety Scenario Modeling for Geological CO_2 Sequestration at Basin Scale: A Case Study of the Taixi Basin (Ph.D. thesis). National Taiwan University.
Kang, X., Li, S., Li, Y., Hu, Z., 1995. Study on the geothermal characteristics and thermal history of Beibuwan basin. J. Jilin Univ. (Earth Sci. Edition) 25, 173–177.
Koide, H., Tazaki, Y., Noguchi, Y., Nakayama, S., Iijima, M., Ito, K., Shindo, Y., 1992. Subterranean containment and long-term storage of carbon dioxide in unused aquifers and in depleted natural gas reservoirs. Energy Convers. Manage. 33, 619–626.
Lei, Z., Zhang, L., Luo, S., et al., 2016. Depositional characteristics and hydrocarbon potential of paleogene in jiulongjiang sag. In: Natural Gas Professional Committee of Chinese Petroleum Society and Sichuan Petroleum Society (Ed.), Proceedings of 2016 National Natural Gas Academic Conference. Guangzhou Marine Geological Survey, China Geological Survey; Key Laboratory of Marine Mineral Resources, Ministry of Land and Resources, Guangzhou, China, pp. 79–89.
Li, J., 2025. Accelerating the offshore CCUS to carbon-neutral China. Fundam. Res. 5, 716–728.
Li, H., Gao, Y., Wang, W., Chen, C., Huang, H., 2014. Experimental study on mineralization storage mechanism of CO_2 in saline aquifers of nanpu depression. J. Northeast. Pet. Univ. 38, 94–102.
Li, C., Tien, N., Zhang, K., Jen, C., Hsieh, P., Huang, S., Maggi, F., 2013. Assessment of large-scale offshore CO_2 geological storage in western Taiwan basin. Int. J. Greenh. Gas. Con. 19, 281–298.
Li, G., Xu, B., Liu, L., 2007. Characteristics of source rocks and conditions for natural gas accumulation in the Taixi basin. Nat. Gas Ind. 27 (5), 48.
Li, X., Yuan, W., Bai, B., 2016. A review of numerical simulation methods for geomechanical problems induced by CO_2 geological storage. Rock Soil Mech. 37 (11).
Lin, A., Watts, A., Hesselbo, S., 2003. Cenozoic stratigraphy and subsidence history of the south China sea margin in the Taiwan region. Basin Res. 15, 453–478.
Lin, D., Xu, W., Lin, Z., Cai, Y., Yang, Y., Chen, X., 2023. Geological CO_2 sequestration: Carbon reduction opportunities and challenges in Taiwan. J. Civ. Hydraul. Eng. 50 (6), 79–86, In Chinese.
Lintong, J., Tianran, M., Cai, L., et al., 2024. Modeling and numerical study of fault activation and fluid leakage induced by CO_2 geological storage. Acta Geol. Sin. 98 (11), 3418–3432.
Litynski, J., Klara, S., McIlvried, H., Srivastava, R., 2010. The United States department of energy's regional carbon sequestration partnerships program: A collaborative approach to carbon management. Environ. Sci. Technol. 44, 15–21.
Liu, J., Lin, C., Li, S., 2020. Neogene tectonic subsidence and depositional systems in the Minjiang-Guangdong coastal basin. Mar. Pet. Geol. 122, 104663.
van der Meer, L.G.H., 1992. Investigations regarding the storage of carbon dioxide in aquifers in the Netherlands. Energy Convers. Manage. 33, 611–618.
Michael, K., Golab, A., Shulakova, V., Ennis-King, J., Allinson, G., Sharma, S., Aiken, T., 2010. Geological storage of CO_2 in saline aquifers—A review of the experience from existing storage operations. Int. J. Greenh. Gas. Con. 4 (4), 659–667.
Nagel, S., Castelltort, S., Wetzel, A., Willett, S., Mouthereau, F., Lin, A., 2013. Sedimentology and Foreland Basin paleogeography during Taiwan arc continent collision. J. Asian Earth Sci. 62, 180–204.
Qin, C., Xiao, G., Wang, J., Liu, Y., 2012. A review of CO_2 storage technology and perspective of CO_2 storage in the nearshore area of South China. Mar. Geol. Front. 28, 40–45.
Qiu, W., 2009. Oligocene to pleistocene basin development and sequence stratigraphy in Northwest taiwan. Master's thesis. Institute of Geophysics, National Central University.
Qiu, N., Li, H., Ding, Z., 2020. Distribution characteristics of geothermal fields and tectonic-thermal evolution in China's offshore basins. Chin. J. Geophys. 63 (5), 1927–1942.
Ru, K., 1990. Half-Graben analysis of rift basins. China Offshore Oil Gas (Geology) 4 (6), 1–10.
Schrag, D., 2009. Storage of carbon dioxide in offshore sediments. Sci. 325 (5948), 1658–1659.
Society of Petroleum Engineers, 2017. CO_2 Storage Resources Management System. Tech. Rep, Society of Petroleum Engineers, Richardson, Texas.
Su, Y., Liu, X., Ji, J., Ma, X., 2021. Role of economic structural change in the peaking of China's CO_2 emissions: An input–output optimization model. Sci. Total. Environ. 761, 143306.
Szulczewski, M., MacMinn, C., Herzog, H., Juanes, R., 2012. Lifetime of carbon capture and storage as a climate-change mitigation technology. Proc. Natl. Acad. Sci. 109, 5185–5189.
Taiwan CPC Corporation, 2019. Structural analogues for CO_2 storage: Lessons from the Taixi basin. In: Proceedings of the 14th Asian Petroleum Geology Symposium. Kuala Lumpur, Malaysia, pp. 112–125.
Teng, L., 1990. Geotectonic evolution of late cenozoic arc-continent collision in Taiwan. Tectonophys. 183, 57–76.
Thibeau, S., Adler, F., 2023. Pressure-derived storage efficiency for open saline aquifer CO_2 storage. Geoenergy 1 (1), geoenergy2022–003.
U.S. Department of Energy, 2007. Carbon Sequestration Atlas of the United States and Canada. National Energy Technology Laboratory.
U.S. Department of Energy, 2008. Carbon Sequestration Atlas of the United States and Canada: Second Edition. Tech. Rep, U.S. Department of Energy.
U.S. Department of Energy, 2010. Carbon Sequestration Atlas of the United States and Canada: Third Edition. Tech. Rep, U.S. Department of Energy.
U.S. Department of Energy, National Energy Technology Laboratory, 2010. Site Screening, Selection and Characterization for Storage of CO_2 in Deep Geologic Formations. Technical Report, (DOE/NETL-2010/1427), Pittsburgh, PA, Designated as 2010b in related publications.
Vangkilde-Pedersen, T., Anthonsen, K., Smith, N., Kirk, K., Neele, F., van der Meer, B., Le Gallo, Y., Bossie-Codreanu, D., Wojcicki, A., 2009. Assessing European Capacity for Geological Storage of Carbon Dioxide. Technical Report, EU GeoCapacity Project.
Wang, H., Zheng, Y., Wang, W., 2022. The major work and implication of geoscience Australia on geological carbon sequestration. Geol. China 49 (3), 1005–1008.
Wei, Z., Zhang, L., Shuai, Q., Yi, H., Qian, X., Lei, Z., Wang, Y., 2018. Application of balanced cross section technique to the study of tectonic evolution of western Taiwan strait basin. Mar. Geol. Quat. Geol. 38 (5), 193–201.
Wu, S., 1991. Evaluation of hydrocarbon plays in eastern China. Pet. Explor. Dev. 3, 1–6.
Xie, K., Huang, D., 2003. Stratigraphic sequence of the tertiary in Taiwan. Taiwan Min. 55 (2), 17–32, In Chinese with English abstract.
Xue, Y., Li, S., Liu, X., Suo, Y., Dai, L., Yu, S., Zhao, S., Wang, P., Xiong, L., An, H., Cheng, S., Wang, X., Ma, Y., 2012. Segmentation of subduction system in the eastern South China sea and dynamics of related basin groups. Mar. Geol. Quat. Geol. 32 (6), 129–147.
Yang, Y., Shuai, Q., Luo, W., Wang, X., 2018. An analysis of the formation and evolution process in the western depression of the Taiwan strait basin by using the equal thickness method. Shandong Chem. Ind. 47 (6), 105–108, In Chinese with English abstract.
Yu, H., Chou, Y., 2001. Characteristics and development of the flexural forebulge and basal unconformity of western Taiwan Foreland Basin. Tectonophys. 333, 277–291.
Yu, H., Huang, F., 1994. Stratigraphy of cenozoic sequences in Taiwan strait and southern East China sea. Pet. Geol. Taiwan 29, 171–192.
Yu, C., Lei, S., Chiao, C., Hwang, L., Yang, W., Yang, M., 2017. Injection risk assessment for intra-formational seal geological model in a carbon sequestration application in Taiwan. Greenh. Gases: Sci. Technol. 7, 225–240.
Zhang, L., Lei, Z., Xu, H., Shuai, Q., Luo, S., Qian, X., 2019a. Sedimentary features and geological conditions for hydrocarbon generation and accumulation in Taixi Basin. Oil & Gas Geol. 40 (1), 152–161.
Zhang, L., Lei, Z., Xu, H., et al., 2019b. Sedimentary characteristics and hydrocarbon generation-accumulation conditions in the Taiwan Western Basin. Oil & Gas Geol. 40 (1), 10.
Zhou, Q., Birkholzer, J., Tsang, C., 2008a. A semi-analytical solution for large-scale injection-induced pressure perturbation and leakage in a laterally bounded aquifer. Water Resour. Res. 44.

Zhou, Q., Birkholzer, J.T., Tsang, C.-F., Rutqvist, J., 2008b. A method for quick assessment of CO_2 storage capacity in closed and semi-closed saline formations. Int. J. Greenh. Gas Con. 2 (4), 626–639, TCCS-4: The 4th Trondheim Conference on CO_2 Capture, Transport and Storage.

Zhou, D., et al., 2011. CO_2 storage potential evaluation of the Pearl River Mouth Basin: A case study for deep saline aquifers in South China Sea. J. Asian Earth Sci. 42, 305–312.